Journal of Electrical Engineering, Electronics, Control and Computer Science – JEEECCS, Volume 10, Issue 37, pages 7-14, 2024

Thermo-Energetic Investigations on a Fitness Bracelet

1st Teoc Alexandru Emanuel
Research grant student in Applied Electronics
"1 Decembrie 1918" University of Alba Iulia
Alba Iulia, Romania
teoc.alexandru.ea21@uab.ro

2nd Tulbure Adrian
Department of Computer Science and Engineering
"1 Decembrie 1918" University of Alba Iulia
Alba Iulia, Romania
aditulbure@uab.ro

3rd Avram Alexandru
Department of Computer Science and Engineering
"1 Decembrie 1918" University of Alba Iulia
Alba Iulia, Romania
alex.avram@uab.ro

Abstract – The increasing popularity of fitness bracelets has led to widespread use of wearable technology for health monitoring. This study examines the thermo-energetic performance of fitness bracelets, focusing on thermal management and energy consumption. The study explores the thermal behavior and energy efficiency of the device, providing insights into the challenges of compact design and continuous operation. These findings aim to guide the optimization of future wearable devices, enhancing both performance and user experience.

Keywords- component; wearable; investigation; analysis; energy consumption; thermal management; measurements

I. INTRODUCTION

In recent years, wearable devices have seen rapid growth, with a variety of body-worn electronic devices such as smartwatches, smart bands, smart glasses, and smart goggles becoming increasingly popular. Among these, fitness bracelets have emerged as some of the most sought-after devices. This growth is driven by ongoing research and development, as well as advancements in flexible and stretchable electronics, which are expanding the potential applications for these devices in consumer, health, biomedical, and industrial sectors [1]. These compact, multifunctional gadgets monitor various physiological parameters. As consumer demand increases, manufacturers have flooded the market with a growing range of options [2]. Despite their popularity, fitness bracelets are complex devices, comprising a multitude of components, including sensors, processors, batteries, and displays, all packed into compact casings.

The increasing density of components in compact devices has raised concerns about their thermal and energy performance. As these devices operate continuously, effective thermal management and heat dissipation have become critical factors for both user comfort and device longevity. With the challenge of maintaining optimal temperatures in ever-shrinking spaces, managing heat is now a key determinant of device efficiency and performance [3]. This study focuses on the thermo-energetic behavior of a fitness bracelet, examining how its design and components perform.

This investigation began with a personal ambition: to design our own monitoring bracelet tailored to meet specific functional and ergonomic requirements. Leveraging advanced Computer-Aided Design (CAD) and Computer-Aided Engineering (CAE) software, I was able to conceptualize and virtually test a prototype that met the desired specifications.

However, due to the complexity and cost of manufacturing such a device, the production phase remained out of reach. Determined to pursue this line of inquiry, I turned my attention to the market, selecting an existing fitness bracelet for in-depth investigations. By studying its design, thermal performance, and energy efficiency, I aimed to bridge the gap between theoretical modeling and practical implementation, gaining insights that could inform future iterations of wearable technology.

II. CONFIGURATION, DESIGN AND WORKING PRINCIPLES

A. Project Specification

Requirements analysis is the first essential step in designing any electronic device. This involves understanding the device's purpose, goals, and specifications, and defining its desired functionalities. Key factors include identifying performance parameters, power requirements, communication protocols, size constraints, and ensuring compliance with relevant industry or regulatory standards [4]. The

process is illustrated in a block diagram, as presented in Figure 1.

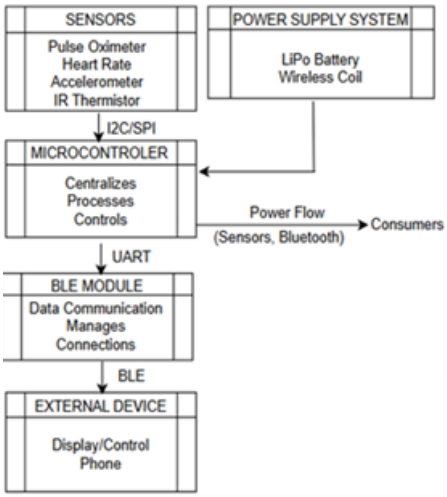

Figure 1. Block Diagram of the operating principle

The device operates by using embedded sensors to measure heart rate in real time. The microcontroller processes data, which is then wirelessly transmitted via Bluetooth to a paired device like a smartphone or tablet, where it is displayed, and alerts are generated if needed. The device is powered by a rechargeable battery.

B. Component selection and Design

The second step is component selection, which involves choosing electronic components based on factors like functionality, size, and performance. This process includes evaluating compatibility, power requirements, and reliability to ensure the components meet the device's needs [4]. In Table I, a detailed Bill of Materials (BOM) is provided, listing the components utilized in the project.

TABLE I. BRACELET COMPONENTS

Component	Description
1. Microcontroller	DA14580
2. Sensors	
b. Accelerometer	BMA421
d. Heart Rate Sensor	PAH8001
3. Bluetooth Module	Not needed separately
4. Power Supply	
a. Lithium Polymer Battery	$3.7V$ / $110mAh$ LiPo
b. Charging Module	Adafruit Qi Receiver
5. Capacitors	
a. Capacitor (0603)	$10nF$ Ceramic Capacitor
b. Capacitor (0402)	$100nF$ Ceramic Capacitor
c. Capacitor (0603)	$4.7\mu F$ Ceramic Capacitor
d. Capacitor (0402)	$1pF$ Ceramic Capacitor
6. Inductors	
a. Inductor (0402)	$1.1nH$ Inductor
b. Inductor (0402)	$10nH$ Inductor
c. Inductor (0603)	$10\mu H$ Inductor
7. Resistors	
a. Resistor (0402)	$10K$ Resistor
b. Resistor (0402)	$3.83K$ Resistor
c. Resistor (0402)	$4.7K$ Resistor

In the schematic design phase, a high-level diagram is created to connect all components, ensuring the circuit meets functional requirements like sensor integration, data transmission, and power management. Following this, the schematic is translated into a physical layout for the Printed Circuit Board (PCB), where components are placed efficiently and compactly. The ergonomic design of the fitness bracelet is also considered to ensure that the PCB fits seamlessly within the housing [4].

Finally, fabricate a prototype PCB based on the design Figure 2, conduct testing to verify functionality, such as sensor performance, wireless connectivity, and battery charging efficiency.

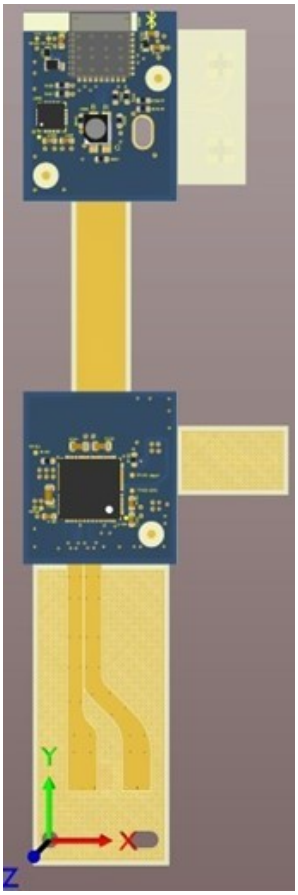

Figure 2. Generated 3D Model

C. Prototype specifications.

To initiate the thermo-energetic investigation, a commercial product was selected as the prototype: the Xiaomi Mi Band 3, a fitness bracelet from the Chinese manufacturer Xiaomi. This device was chosen due to its widespread use and relatively accessibility, providing a suitable platform for analyzing the thermal and energy performance of wearable technology. The Xiaomi Mi Band 3 is equipped with features and sensors, which include: (Xiaomi Corporation, 2018) [5].

- **Display**: $0.78 - inch$ Organic Light-Emitting Diode (OLED) touch screen, capable of displaying basic information and notifications.
- **Sensors**:
  - *Heart Rate Sensor*: Optical heart rate sensor for continuous monitoring of heart rate during physical activities.
  - *Accelerometer*: Measures motion and detects activity patterns, supporting features like step counting and sleep tracking.

- **Battery**: 110 mAh Lithium Polymer (LiPo) battery, providing a long- lasting power source.
- **Connectivity**: Bluetooth 4.2 Low Energy (LE) for communication with external devices such as smartphones.
- **Water Resistance**: Ingress Protection (IP67) - rated, allowing the device to withstand immersion in water up to 1 $meter$ for 30 $minutes$.

These features make the Xiaomi Mi Band 3 a relevant example for evaluating the thermo-energetic characteristics of wearable fitness technology.

III. Experimental Studies

This chapter details the methodologies used in investigating the thermo-energetic characteristics of the fitness bracelet. The primary aim was to comprehensively evaluate the operational parameters, structural design, and thermal behavior under varying functional states.

A. Disassembly and Component investigation

To understand the internal structure and operational principles of the fitness bracelet, the first step involved careful disassembly. To facilitate this process and ensure the device remained functional during the investigation, I made some modifications by extending the connection wires to the battery, allowing for greater flexibility during disassembly. Figure 3 illustrates the disassembled sections of the bracelet device, including the battery, casing, and printed circuit board (PCB).

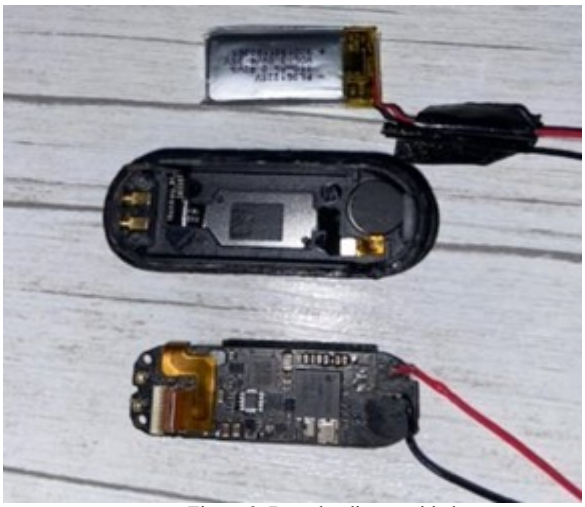

Figure 3. Bracelet disassembled

This process was executed with precision to avoid damaging the delicate components. The internal architecture revealed the main components responsible for the device's functionality.

B. Functional Feature Assessment

Following the disassembly, the functional features of the bracelet were systematically analyzed. Key functionalities such as heart rate monitoring, step counting, and Bluetooth connectivity were evaluated to establish a baseline of operations. This phase ensured a clear understanding of the interplay between hardware and software, which was essential for correlating thermal behavior with specific activities.

The primary focus of this experimental study was to investigate the thermal characteristics of the bracelet under various operational states.

Using a Caterpillar S62 Pro equipped with FLIR's VividIR technology Infrared (IR) camera [6], the surface temperatures of the device were measured. The IR camera allowed precise identification of thermal hotspots on the PCB and other critical areas. The following operational modes were analyzed:

1) Active Mode: The bracelet was powered on and functioned at a standard operational level, including basic step counting and Bluetooth standby.

2) Active with Chronometer: The bracelet was set to active mode with the chronometer feature enabled.

3) Active with Chronometer and Heart Rate Sensor: The more demanding operational mode was tested by enabling both the chronometer and continuous heart rate monitoring.

C. Termal Investigation

In a room-temperature environment, during active standby mode, Figure 4 illustrates the temperature distribution on the front of the uncovered PCB with the display. A hotspot is observed in the bottom-left corner, where the temperature reaches $31.8°C$, while the rest of the board exhibits temperature variations ranging from $23.6°C$ to $25.2°C$. The hotspot is identified as the connector associated with the heart rate monitoring sensor. Although the sensor is inactive currently, an increase in temperature is still detected in this area.

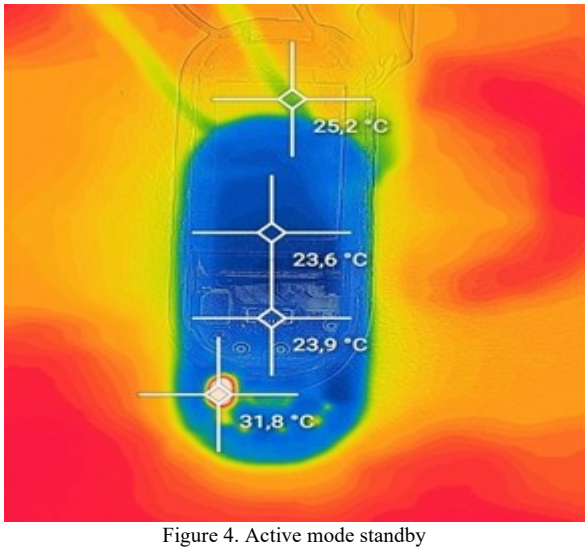

Figure 4. Active mode standby

Figure 5 illustrates the second operating mode, which corresponds to the active mode with a chronometer function. In this test, the chronometer on the bracelet was activated with the display enabled, and the device was left operating for approximately 40 $minutes$ in the same room-temperature environment. The results indicate a significant overall temperature increase across the PCB, with temperatures rising by $3°C$ to $8°C$ throughout the board.

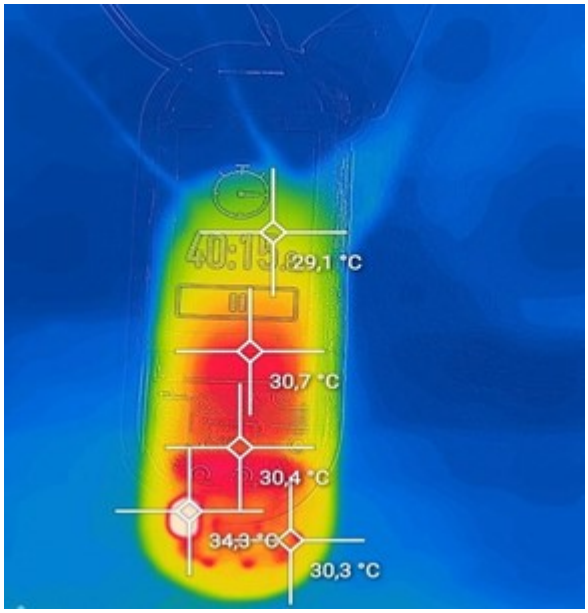

Figure 5. Active mode chronometer

The final analysis conducted on the front of the device focused on the mode with Chronometer and Heart Rate Sensor active Figure 6. In this mode, the heart rate sensor was activated to perform measurements, resulting in increased energy consumption. The most significant temperature change was located at the sensor connector, reaching a maximum temperature of $35.4°C$.

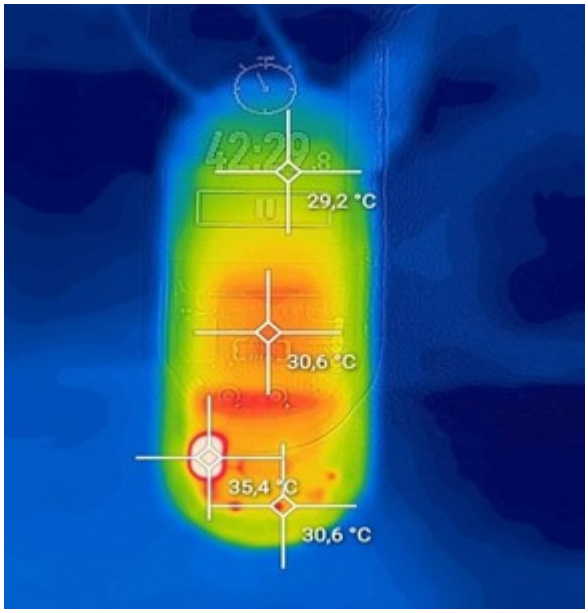

Figure 6. Active mode heart rate sensor monitoring

The investigation continues with an analysis of the internal device temperatures, illustrating the temperature distribution during active mode.

This analysis provides baseline measurements, as shown in Fig. 7, which serves as a reference level for further evaluations. Understanding these temperature profiles is essential for assessing the device's performance and for improvement.

In the following images, captured after the previous mode in which all systems were active, several points of significant heat generation have been identified. These points are highlighted by the temperature indicators placed on the images to monitor and track the heat distribution.

The primary internal hotspots have been identified. In the top-left corner, above the DA14580 microcontroller, a component is observed to produce more heat, starting at a temperature of $27.5°C$ in Figure 7 and reaching a peak of $33.3°C$ in Figure 8. This component has been identified as a $16\,MHz$ crystal oscillator.

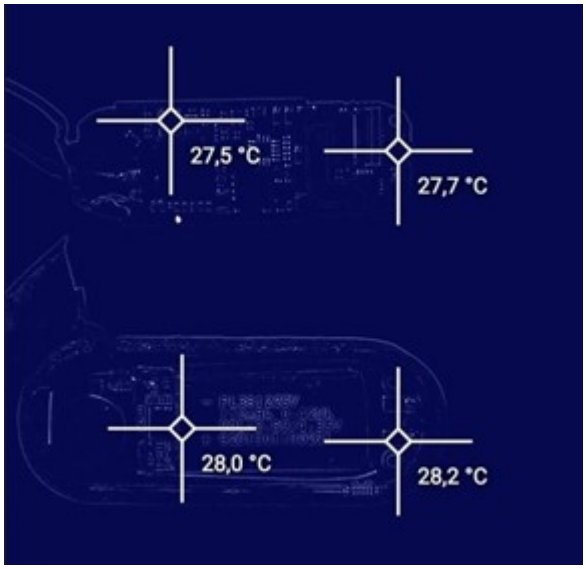

Figure 7. Thermal image capture (standby)

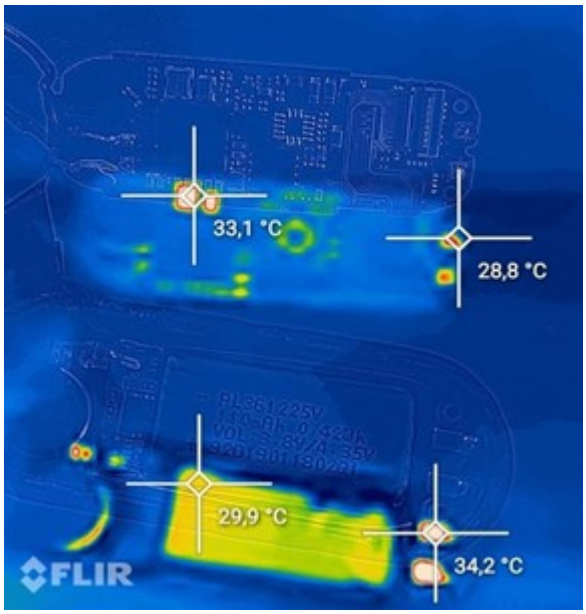

Figure 8. Thermal image capture (initial state)

The second notable hotspot is located in the bottom-right corner, where two distinct points are more clearly visible. These points exhibit temperatures starting at $28.2°C$ in Figure 7 and peaking at $34.2°C$ in Figure 8, and they have been identified as the charging connectors.

In Figure 9, the intermediate state of the internal temperatures of the components is presented.

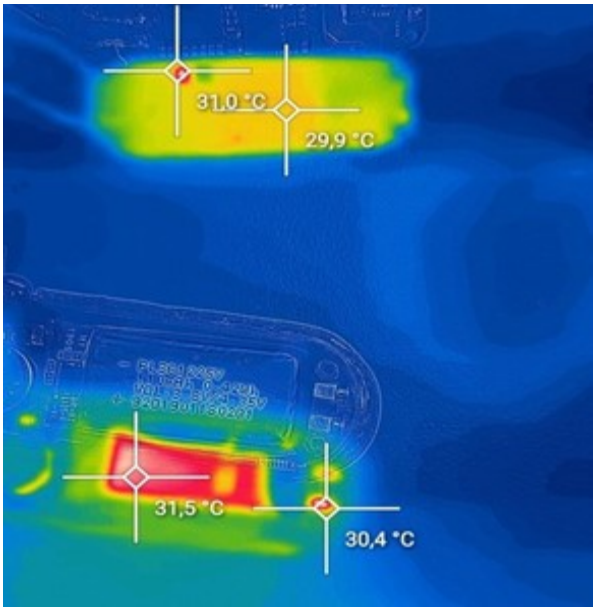

Figure 9. Thermal image capture (middle state)

The final hotspot is observed on the left side of the battery itself, which exhibits an increase in temperature from $28.0°C$ in Figure 7 to a peak of $32.4°C$ in Figure 10. These represent the main hotspots identified on the Device Under Test (DUT).

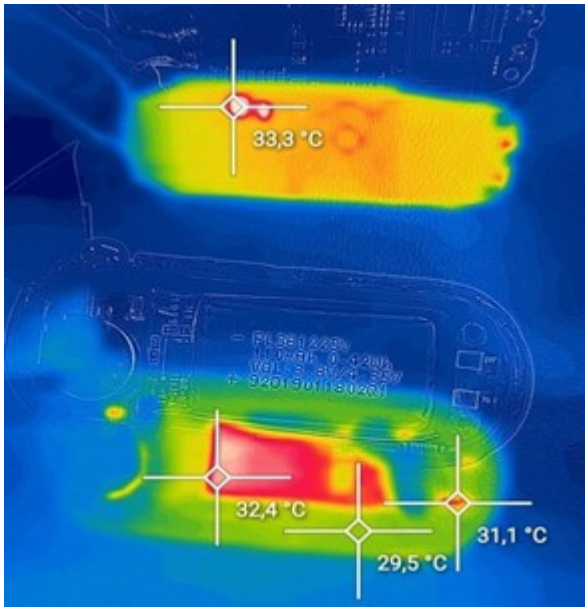

Figure 10. Thermal image capture (final state)

All this information, together with the thermally relevant coefficients, has been summarized in Tables II and III.

So, in Table II is given the temperature evolution over time for some components (accessible to measure). And in Table III the data sheet of the investigated components. With sample 1 up to 7 are indicated the thermal captures taken at the time intervals indicated in seconds.

TABLE II. TEMPERATURE EVOLUTION ON COMPONENT SURFACES

Time [s]	**Components temperature [°C]**		
	Connector	***OSC***	***Battery***
Ambient Temp.	25,7	25,7	25,7
sample1 34: 26	29,1	27,5	28,0
sample2 36: 09	32,5	–	–
sample4 40: 02	33,3	31,0	31,5
sample5 40: 15	34,3	–	–
sample6 42: 22	35,3	–	–
sample7 42: 29	35,4	33,3	32,4
Temp. $\Delta T\ [\ Grad]$	9,7	7,6	6,7

TABLE III. COMPONENTS CHARACTERISTICS

Charac.	**Components data**		
	Connect.	***OSC.***	***Battery***
Dimensions $(L \times l \times H)$	$3 \times 2 \times 1$	$3{,}2 \times 2{,}5 \times 0{,}6$	$30 \times 35 \times 5.0$
Active surface (mm^2)	16,00	14,84	1050
Mass $[g]$	0,015	0,020	10
Active material Type	plastic stainless steel	Quartz Ceramic package	$LiCoO_2$ Graphite Com. gel polymer
Specific heat c $\left[\frac{J}{g \cdot K}\right]$	$0{,}63 - 0{,}7$	$0{,}42 - 0{,}65$	0,84
Convectiv transfer coef. αcv $\left[\frac{W}{m^2 \cdot K}\right]$	$2{,}5 \cdot \Delta T^{0{,}25}$	$2{,}5 \cdot \Delta T^{0{,}25}$	$2{,}5 \cdot \Delta T^{0{,}25}$

The material constant "specific heat capacity" is the quantity of heat required per mass unit of a body to change its temperature by one degree. The convective heat transfer coefficient (αcv) depends on the fluid properties and the physical situation. In the present study only the convective heat transfer coefficient for laminar flow was considered.

In operation mode, the energy losses are converted into heat. This is partly stored in the analyzed components Q_a and partly delivered by convection Q_{cv} according to (1) or after integration, acc. to (2):

$$\int_0^t u \cdot i \cdot dt = C_{th} \cdot (T - T_a) + \int_0^t D \cdot (T - T_a) \cdot dt \quad (1)$$

$$u \cdot i \approx mc \cdot \frac{dT}{dt} + D \cdot (T - T_a) \quad (2)$$

$$D = \alpha cv \cdot A \quad (3)$$

Where: αcv = transfer coefficient and
A = component surface

D. Electrical Investigation

Electrical investigation is crucial to our objectives, as analyzing energy consumption enables us to determine power losses in individual components.

In addition to thermal investigations, energy measurements provide a basis for identifying potential solutions for design optimization.

In this case, by extending the supply conductors, a configuration that allowed a voltage and a current probe to be placed on the DUT was adopted. This set-up (Figure 11) enabled accurate measurement of current and voltage using a digital oscilloscope.

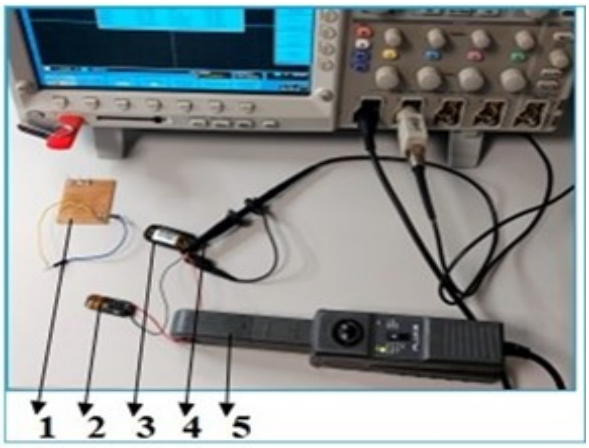

Figure 11. Measurement set-up: 1. Voltage shunt; 2. Electronic board; 3. Battery housing; 4. Voltage probe; 5. Current probe

A passive probe offering adequate ruggedness and wide dynamic range was used to measure the supply voltage level [7]. For current measurement purposes a long nose style Clamp Probe (CP) uses hall effect current sensor to provide voltage output to oscilloscopes. The main characteristics and settings are shown in Figure 12.

Figure 12. Current probe characteristics

The waveform of the measured signals is plotted graphically (Figure 13) and numerically (Table IV) in the adjacent pictures. The acquisition rate is sampled at 500 $ksample/sec$ on both channels, and the display was done by averaging the values at 2 $msec$.

The power absorbed by the bracelet was determined by mathematical calculations within a total interval of 50 $msec$ (last column, Table IV).

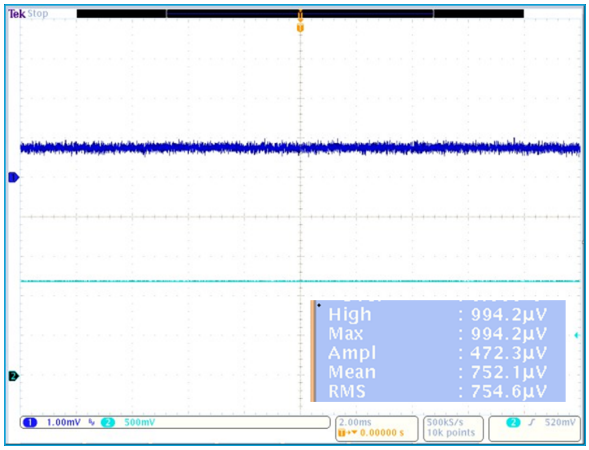

Figure 13. Current (Ch1 – $10mA/div$) and voltage (Ch2 – $500mV/div$) oscillograms

From the above oscillogram, it can be seen, that depending on the operating mode, the bracelet board absorbs the following voltage and current values:

$$I_{abs\cdot avg} = 7{,}52\ mA\ (\approx 752{,}1\ \mu V)$$

$$I_{abs\cdot max} = 9{,}94\ mA\ (\approx\ 994{,}2\ \mu V)$$

$$U_{abs.avg} = 1{,}21\ V$$

TABLE IV. NUMERICAL POWER CONSUMPTION (2ms SAMPLE) $Avg.power = 9{,}138\ mW$

Time[sec]	I[mA]	U[V]	P[mW]
0	7,2297	1,2046	8,7090
0,002	6,9484	1,202	8,3517
0,004	6,8625	1,2039	8,2618
0,006	7,5141	1,2005	9,0204
0,008	7,9281	1,1995	9,5094
0,01	6,7141	1,2002	8,0579
0,012	7,5750	1,2088	9,1563
0,014	7,9156	1,1996	9,4957
0,016	6,7141	1,2041	8,0841
0,018	8,4328	1,2025	10,1405
0,02	7,8375	1,2016	9,4179
0,022	6,6031	1,1984	7,9135
0,024	7,8297	1,2028	9,4176
0,026	7,4328	1,1985	8,9084
0,028	7,9406	1,2009	9,5356
0,03	7,6422	1,2016	9,1825
0,032	8,0781	1,2088	9,7644
0,034	7,3953	1,2002	8,8756
0,036	7,8016	1,2083	9,4265
0,038	8,2563	1,2027	9,9295
0,04	8,0797	1,202	9,7114
0,042	7,8719	1,1981	9,4315
0,044	7,4438	1,2023	8,9494
0,046	8,2984	1,2007	9,9639
0,048	7,7141	1,1988	9,2472
0,05	8,1234	1,1994	9,7431

Conclusions & Discussion

Generated heat in equipment leads to shortening of the DUT lifespan, limits its performance and often generate failure in the electronic systems. The correct choice of cooling mode avoids many negative effects.

The heat dissipation systems differ primarily in size, but also in cooling medium or dissipation efficiency. Table V shows, exemplary, the dissipated heat in some relevant components.

In the analyzed period $dt = 42{,}29\ min \approx 2549\ s$. (End time, Figure 6.) the bracelet consumption was $E_{end} = 23{,}29Ws = 100\%$. This energy is dissipated both on the 2 loads from Table V, as:

- stored heat (load 1+2): $Qa = 172{,}02\ mWs$
- convectiv heat (load $1 + 2$): $Qcv = 2.938{,}73\ mWs$

In total $3{,}11\ Ws$, which means $\approx 13\%$ of total consumption. The difference of 87% of the entire energy will dissipate on other loads from Table I.

TABLE V. ENERGY CONSUMPTION AND HEAT CONVERSION

Charact.	Comp.		
	load 1 connector	***load 2 oscillator***	***source battery***
Active mode *dt* $[sec]$	2.549		$1512Ws*$
Power supply *P* $[mW]$	9,14		
Total energy *E* $[mWs]$	23.297,86		
Internal stored heat *Qa* $[mWs]$	97,59	74,48	56.451,97
Convectiv heat *Qcv* $[mWs]$	1.745,40	1.193,33	75.064,86

By the analyzed DUT, a reduction of power losses could be obtained by appropriate design measures [8]. Following the investigations, three optimization methods were identified, namely:

1) Repositioning of the main connector (Figure 14. top) from horizontal to vertical, for better heat dissipation and increasing the coefficient αcv like below [9]. This means that approx. 60% more heat can be dissipated.

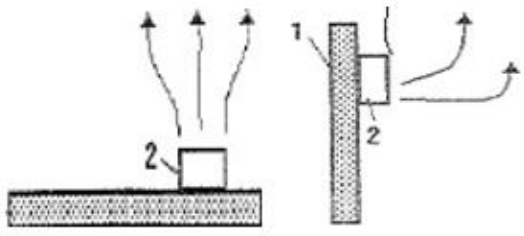

Figure 1. Heat convection coefficient in space

$$\alpha cv = 2{,}5 \cdot \Delta T^{0{,}25}\ [W/m^2K\ ]$$
$$\alpha cv = 4{,}2 \cdot \Delta T^{0{,}25}\ [W/m^2K]$$

2) Decreasing the oscillator frequency, or if necessary, implementing a frequency divider leading to lower switching losses Ps, with ca. 30%, according to the calculation formula below (4):

$$P_s = f_s \cdot (\int_{Ton} p(t) \cdot dt + \int_{Toff} p(t) \cdot dt) = \\ = f_s \cdot (E_{on} + E_{off}) \quad (4)$$

3) increasing the convection surface area (Acv) by bonding/welding ribs or tubes on the heat exchange surfaces (depending on the component location).

In this study the phenomena like evaporation and radiation transfers heat were neglected.

REFERENCES

[1] U. N. C. on T. and Development, UNCTAD Annual Report 2022. 2023.

[2] "Highlights Annual Report 2023-Port of Rotterdam Authority".

[3] M. Stopford, "Maritime Economics, 3rd ed. New York: Routledge.," Choice Reviews Online, vol. 47, no. 07, pp. 47-3934-47–3934, 2010.

[4] E. Lindstad and T. I. Bø, "Potential power setups, fuels and hull designs capable of satisfying future EEDI requirements," Transp Res D Transp Environ, vol. 63, pp. 276–290, Aug. 2018, doi: 10.1016/J.TRD.2018.06.001.

[5] L. Li, H. Hong, J. Cao, and Y. Yang, "Progress in Marine Antifouling Coatings: Current Status and Prospects," Coatings 2023, Vol. 13, Page 1893, vol. 13, no. 11, p. 1893, Nov. 2023, doi: 10.3390/COATINGS13111893.

[6] Z. Fu et al., "Fuel cell and hydrogen in maritime application: A review on aspects of technology, cost and regulations," Sustainable Energy Technologies and Assessments, vol. 57, p. 103181, Jun. 2023, doi: 10.1016/J.SETA.2023.103181.

[7] G. J. Grigoropoulos, "Hull form optimization for hydrodynamic performance," Marine Technology and SNAME News, vol. 41, no. 4, pp. 167–182, 2004, doi: 10.5957/MT1.2004.41.4.167.

[8] "Improving the energy efficiency of ships." Accessed: Nov. 14, 2024. [Online]. Available: https://www.imo.org/en/OurWork/Environment/Pages/Improving%20the%20energy%20efficiency%20of%20ships.aspx

[9] P. Pan, Y. Sun, C. Yuan, X. Yan, and X. Tang, "Research progress on ship power systems integrated with new energy sources: A review," Renewable and Sustainable Energy Reviews, vol. 144, p. 111048, Jul. 2021, doi: 10.1016/J.RSER.2021.111048.